Palynological evidence for a southward shift of the North Atlantic Current at ~2.6 Ma during the intensification of late Cenozoic Northern Hemisphere glaciation

Jan A. I. Hennissen[1,2], Martin J. Head[1,3], Stijn De Schepper[4,5,6,7], and Jeroen Groeneveld[6]

[1]Department of Earth Sciences, University of Toronto, Toronto, Ontario, Canada, [2]Now at British Geological Survey, Keyworth, UK, [3]Department of Earth Sciences, Brock University, St. Catharines, Ontario, Canada, [4]Department of Earth Science, University of Bergen, Bergen, Norway, [5]Department of Geosciences, University of Bremen, Bremen, Germany, [6]Now at Uni Research Climate, Bergen, Norway, [7]Bjerknes Centre for Climate Research, Bergen, Norway

Abstract The position of the North Atlantic Current (NAC) during the intensification of Northern Hemisphere glaciation (iNHG) has been evaluated using dinoflagellate cyst assemblages and foraminiferal geochemistry from a ~260 kyr interval straddling the base of the Quaternary System from two sites: eastern North Atlantic Deep Sea Drilling Project Site 610 in the path of the present NAC and central North Atlantic Integrated Ocean Drilling Program Site U1313 in the subtropical gyre. Stable isotope and foraminiferal Mg/Ca analyses confirm cooling near the marine isotope stage (MIS) G7–G6 transition (2.74 Ma). However, a continued dominance of the dinoflagellate cyst *Operculodinium centrocarpum* sensu Wall and Dale (1966) indicates an active NAC in the eastern North Atlantic for a further 140 kyr. At MIS 104 (~2.60 Ma), a profound dinoflagellate cyst assemblage turnover indicates NAC shutdown in the eastern North Atlantic, implying elevated atmospheric pressure over the Arctic and a resulting shift in the westerlies that would have driven the NAC. These findings challenge recent suggestions that there was no significant southward shift of the NAC or the Arctic Front during iNHG, and reveal a fundamental climatic reorganization near the base of the Quaternary.

1. Introduction

The Pliocene Epoch (5.33–2.58 Ma) marks the transition from a stable and warm global climate to a variable one characterized by alternating glacial–interglacial conditions and recurring Northern Hemisphere ice sheets [e.g., *Dowsett and Poore*, 1991; *Raymo et al.*, 2006; *Lisiecki and Raymo*, 2007]. Early late Pliocene sea surface temperatures (SSTs) were 3.5°C higher than today in the midlatitudes of the North Atlantic and even 5–6°C higher in the high latitudes, effectively inhibiting the formation of ice sheets [*Cronin*, 1991; *Dowsett et al.*, 1996, 2009; *Haywood et al.*, 2009]. Paradoxically, around 2.74 Ma, a massive increase of ice-rafted debris (IRD) in Atlantic and Pacific Ocean sediments [*Shackleton et al.*, 1984; *Jansen et al.*, 1988, 2000; *Vorren et al.*, 1988; *Jansen and Sjøholm*, 1991; *Raymo*, 1994; *Kleiven et al.*, 2002; *Naafs et al.*, 2013a] evidences the expansion of Northern Hemisphere ice sheets. Several mechanisms have been proposed to explain this major climatic event: e.g., regional changes across all latitudes [*Ravelo et al.*, 2004], the replacement of a permanent El Niño by the extant Walker circulation [*Cane and Molnar*, 2001] and onset of permanent stratification [*Rea and Schrader*, 1985; *Haug et al.*, 1999; *Sigman et al.*, 2004; *Reynolds et al.*, 2008] in the Pacific Ocean, changes in the dominance of the orbital parameters [*Maslin et al.*, 1998; *Raymo and Nisancioglu*, 2003], a dropdown in pCO$_2$ [*Seki et al.*, 2010], and the emergence of the Panamanian Isthmus [*Driscoll and Haug*, 1998; *Haug and Tiedemann*, 1998; *Bartoli et al.*, 2005].

None of these mechanisms on its own explains conclusively how the intensification of Northern Hemisphere glaciation (iNHG) occurred. Recent studies have focused on the role of the North Atlantic Current (NAC) because it constitutes a vital part of the Atlantic limb of the thermohaline circulation (THC). Coupled ocean–atmosphere models have shown that the NAC transports significant heat and moisture to high latitudes of the Atlantic realm [*Klocker et al.*, 2005; *Lunt et al.*, 2008a, 2008b]. Hence, fluctuations in the strength and position of the NAC should have major repercussions for ice sheet formation. For the late Pliocene to early Pleistocene, *Naafs et al.* [2010] showed a reduced influence of the NAC at Integrated Ocean Drilling Program (IODP) Site U1313 using a combination of alkenone SST reconstructions and alkenone-based surface water
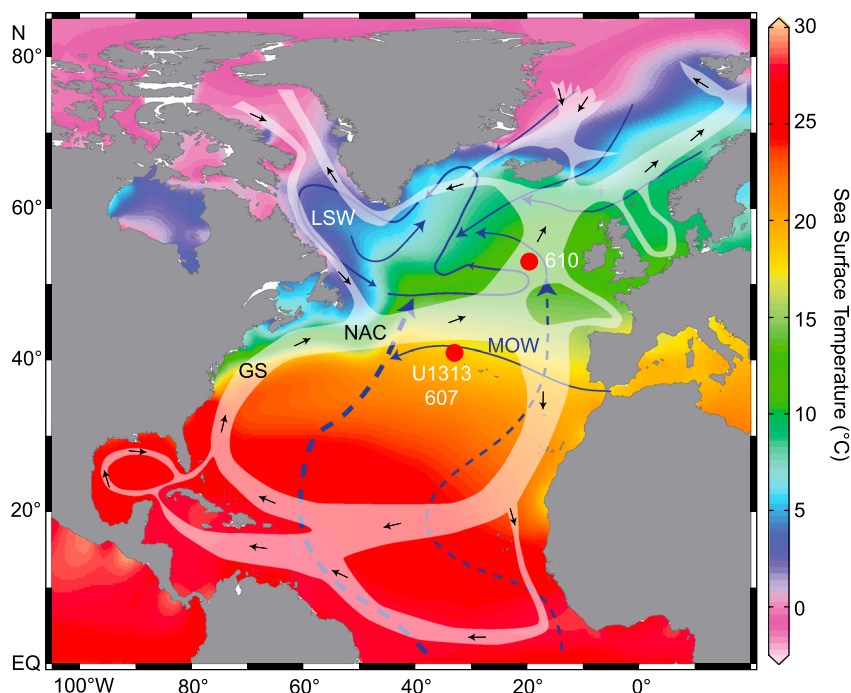
Figure 1. Location of IODP Site U1313 and DSDP Site 610 in the North Atlantic showing the present surface circulation in light shading with black arrows [*Hansen and Østerhus*, 2000], deep-water circulation as blue lines with Antarctic bottom waters as dashed lines [*Stramma*, 2001], and modern sea surface temperatures following *Locarnini et al.* [2010]. GS = Gulf Stream; NAC = North Atlantic Current; MOW = Mediterranean Outflow Water; LSW = Labrador Sea Water. Surface ocean circulation is from Dowsett in *Williams et al.* [2009]. The map was drawn using Ocean Data View [*Schlitzer*, 2011].

productivity. These authors suggested that during Quaternary-style glacials that started during marine isotope stage (MIS) G6 and especially from MIS 100 onward, an almost undeviated west-to-east flow of the NAC directed at around 40°N, developed which was associated with a southward shift of the Arctic Front to the midlatitudes. This view was contested by *Friedrich et al.* [2013] who interpreted high SST$_{Mg/Ca}$ in *Globigerinoides ruber* during early Pleistocene glacials as evidence of a NAC position well north of Site U1313, implying only a modest reduction of heat transport to the high latitudes.

The current paper aims to elucidate the role of the NAC during the iNHG by examining various proxies from a ~260 kyr (2782–2520 ka) time slab that incorporates MIS G6 and the earliest Pleistocene glacials. We integrate marine palynology (dinoflagellate cyst assemblages) and foraminiferal geochemistry (stable isotopes and Mg/Ca paleothermometry) using a same-sample technique [*De Schepper et al.*, 2009, 2013] at millennial-scale resolution. Samples were taken from Deep Sea Drilling Project (DSDP) Hole 610A, currently in the path of the NAC, and IODP Hole U1313C, within the subtropical gyre, forming a latitudinal transect through this crucial part of the North Atlantic.

2. Oceanography

DSDP Hole 610A (53°13′N; 18°53′W; 2417 m water depth; Figure 1) was drilled as part of DSDP Leg 94 [*Ruddiman et al.*, 1987a]. The hole is located on the Feni Drift, a 600 km long and 500 m thick sediment drift [*Dowling and McCave*, 1993] that contains deposits dating back to the early Miocene [*Stoker et al.*, 2005]. IODP Hole U1313C is a reoccupation of DSDP Hole 607 located 400 km northwest of the Azores (41°00′N; 32°57′W; Figure 1) and drilled at a water depth of 3426 m [*Expedition 306 Scientists*, 2006].

The benthos at DSDP Site 610 is mostly influenced by a North Atlantic Deep Water (NADW) and Labrador Sea Water (LSW) mixture as well as by Antarctic Bottom Water (AABW) advected into the Atlantic Basin from the South Atlantic. These two deep-water mixtures can be distinguished by their different δ^{13}C signatures, AABW having lower δ^{13}C values than NADW [*Ravelo and Andreasen*, 2000; *Curry and Oppo*, 2005]. At IODP Site

U1313, beside NADW and AABW, the benthos is influenced by Mediterranean Water entering the Atlantic Basin as a saline plume bounded by the southernmost branch of the NAC [*Sy*, 1988].

The most prominent surface oceanographic feature in the study area is the NAC (Figure 1). Models estimate a northward heat transport of around 0.9 PW by the Gulf Stream–NAC complex [*Ganachaud and Wunsch*, 2000; *Prange and Schulz*, 2004; *Klocker et al.*, 2005]. This heat, combined with a high-salinity flux of 6.5 (±2.20) Sv psu [*Bacon*, 1997], makes the Gulf Stream–NAC complex a key feature of the Atlantic part of the THC. Alongside the THC, wind stress caused by the prevailing westerlies drives the extant NAC around 52° east-northeast across the basin [*McCartney and Talley*, 1982] before it turns northward across the Greenland–Scotland Ridge [*McCartney and Mauritzen*, 2001]. In this way, the Gulf Stream–NAC system forms the western and northern boundary of the North Atlantic anticyclonic gyre (Figure 1) [*Hansen and Østerhus*, 2000].

3. Methods

3.1. Samples and Sample Preparation

From DSDP Hole 610A, we collected 73 samples (15 cm^3) from cores 14 and 15 across the interval 125.74–136.72 m below sea floor (mbsf; supporting information), representing an average sampling distance of 18 cm (3.1 kyr). The sediment consists of nannofossil ooze and calcareous mud with marly and siliceous intervals with only minor, centimeter-scale bioturbations [*Ruddiman et al.*, 1987a].

From IODP Hole U1313C, 95 samples (15 cm^3) were collected from core 13 and core section 14-1, across the interval 107.23–118.04 mbsf (supporting information), representing an average sampling distance of 11 cm (2.5 kyr). The lithology consists of cyclically layered intervals of dark sediment, containing some terrigenous material, and lighter colored sediment, mainly foraminiferal and nannofossil ooze poor in terrigenous material [*Ruddiman et al.*, 1987b; *Expedition 306 Scientists*, 2006].

We extracted dinoflagellate cysts and foraminifers from the same sediment samples following the method of *De Schepper et al.* [2009] as detailed in *Hennissen* [2013]. Palynological processing followed standard procedures as also outlined in *De Schepper et al.* [2009].

3.2. Stable Isotope Analyses on Foraminifer Tests

Benthic stable isotope records ($\delta^{18}O_{benthic}$ and $\delta^{13}C_{benthic}$) for both sites were determined using *Cibicidoides wuellerstorfi* as the biotic carrier. The $\delta^{18}O_{benthic}$ record of Hole 610A was correlated to the orbitally tuned LR04 stack of *Lisiecki and Raymo* [2005] using the lineage routine in Analyseries 2.0.4.2 [*Paillard*, 1996] to obtain the age model. For Hole U1313C, we used the age model of *Bolton et al.* [2010]. The carbon isotopic composition of the benthic foraminifer tests was determined to elucidate the deep-water contribution at the sampled sites, as these organisms incorporate carbon into their tests in approximately the same isotopic ratio as the surrounding water [*Curry et al.*, 1988; *Bartoli et al.*, 2005; *Ravelo and Hillaire-Marcel*, 2007]. To assess sea surface conditions (Mg/Ca-based SST and relative salinity estimates based on $\delta^{18}O$), *Globigerina bulloides* was selected as the biotic carrier because of its cosmopolitan character and tolerance of a broad range of temperatures (between 10 and 20°C) [*Bé*, 1980; *Vincent and Berger*, 1981; *Kucera et al.*, 2005; *Kucera*, 2007]. All stable isotope analyses were carried out at Bremen University on a Finnigan MAT252 mass spectrometer calibrated to NBS 19 [*Coplen*, 1995] with a reproducibility of ±0.08‰ for $\delta^{18}O$ and ±0.04‰ for $\delta^{13}C$, yielding an analytical standard deviation of ±0.02‰ for $\delta^{18}O$ and ±0.01‰ for $\delta^{13}C$. Results are reported in permil versus the Pee Dee belemnite scale.

3.3. Mg/Ca-Derived SST

Variations of the Mg/Ca ratio in the test of *G. bulloides* are well established and calibrated through culturing and core-top studies [*Mashiotta et al.*, 1999; *Elderfield and Ganssen*, 2000]. *Globigerina bulloides* is a spinose foraminifer that occupies the upper 60 m of the water column [*Schiebel et al.*, 1997] in temperate regions [*Pflaumann et al.*, 2003] and above 40°N, its Mg/Ca ratio records average April to June temperatures [*Robinson et al.*, 2008]. About 40 tests per sample were selected for Mg/Ca analysis and subjected to the foraminiferal cleaning procedure described by *Barker et al.* [2003] with the adaptations of *Nürnberg and Groeneveld* [2006]. The Mg/Ca analyses were carried out at Bremen University on an ICP-OES (ISA Jobin Yvon-Spex Instruments GmbH) with a polychromator. For each sample, three replicate analyses were made which yielded an

analytical standard deviation of 0.002 mmol/mol. To obtain an estimate of SST, the acquired Mg/Ca ratios were inserted into the *Elderfield and Ganssen* [2000] algorithm for North Atlantic core-top samples:

$$Mg/Ca = 0.52 \times e^{0.10T} \qquad (1)$$

where *T* is sea surface temperature (°C).

The analytical error for Mg and Ca is 0.93% and 0.12%, respectively, which propagates to 0.09°C using *Elderfield and Ganssen* [2000] (supporting information). However, the effective error is likely to be an order of magnitude higher due to differences in test calcification of the biotic carrier, vital effects, and taphonomic processes, and replicate analyses have shown they amount to as much as 0.8°C [see also *Nürnberg and Groeneveld*, 2006; *De Schepper et al.*, 2009].

3.4. The Isotopic Composition of the Surface Seawater and Relative Salinity Estimates

To calculate the isotopic composition of the surface seawater, we used the empirically derived temperature equation of *Shackleton* [1974] and solved for $\delta^{18}O_{sw}$:

$$\delta^{18}O_{sw} = \delta^{18}O_{planktonic} - 21.9 + 0.27\sqrt{310.6 + (10 \times T)} \qquad (2)$$

where $\delta^{18}O_{sw}$ is the oxygen isotope composition of the surface seawater (‰) and $\delta^{18}O_{planktonic}$ is the oxygen isotope composition of the foraminifer test (‰).

To approximate the impact of global ice volume and global SST on the isotopic composition of the seawater, the normalized benthic $\delta^{18}O$ of the LR04 stack was subtracted from the $\delta^{18}O_{sw}$ record. Doing so corrected the record for both SST and global ice volume, leaving salinity as the main influence on fluctuations of the oxygen isotopic composition of the Pliocene–Pleistocene seawater ($\delta^{18}O_{sw-ice}$). The salinity curves represent relative changes because the exact relationship between salinity and seawater for this time interval is unknown [*Rohling*, 2007].

3.5. Dinoflagellate Cyst Analysis

Microscope slides were examined on a Leica DM2500 microscope at 400X magnification for routine counting, and 1000X for morphological analysis. Samples were counted until 300 dinoflagellate cysts were identified or two entire slides were counted. All encountered acritarchs, pollen, and spores were also tabulated. During the palynological preparation, one *Lycopodium clavatum* tablet (batch no. 177745) was added as a spike in each sample to determine dinoflagellate cyst concentrations using the marker grain method [*Stockmarr*, 1971]. Using the dinoflagellate cyst concentration, a dinoflagellate cyst burial flux (DBF) can be derived:

$$DBF = C \times \rho_{dry} \times S \qquad (3)$$

where DBF is the dinoflagellate cyst burial flux (cysts/(cm^2 kyr)), ρ_{dry} is the salt-free bulk density of the sediment (g/cm^3), and *S* is the sedimentation rate (cm/kyr).

The DBF incorporates sedimentation rate and total dinoflagellate cyst concentration. Hence, when compared to the dinoflagellate cyst concentration, the DBF will distinguish those fluctuations caused by changing sedimentation rates from those reflecting effective changes in dinoflagellate cyst recruitment in the sediment.

4. Results

4.1. Age Models and $\delta^{18}O_{benthic}$

Sixty-three out of 73 samples from Hole 610A yielded enough well-calcified tests from *C. wuellerstorfi* to ensure reproducible benthic oxygen isotope analysis (supporting information). The $\delta^{18}O_{benthic}$ record fluctuates between 2.01‰ (131.21 mbsf) and 3.70‰ (132.56 mbsf; Figure 2). Graphic correlation of this record with the LR04 stack constrained the record from 2782 to 2565 ka, for a total duration of 217 kyr across a depositional thickness of 10.98 m (Figure 2). This translates to an average sedimentation rate of 5.2 cm/kyr, with extremes of 1.5 cm/kyr during MIS 104 and 10.7 cm/kyr around MIS 103–102 (Figure 2). This is similar to the DSH08 age model [*De Schepper and Head*, 2008].

In Hole U1313C, the benthic $\delta^{18}O$ record varies from 2.16‰ (at 112.98 mbsf; 2657 ka) to 3.94‰ (at 107.46 mbsf; 2525 ka; supporting information). To allow direct comparison with other SST and stable isotope records,
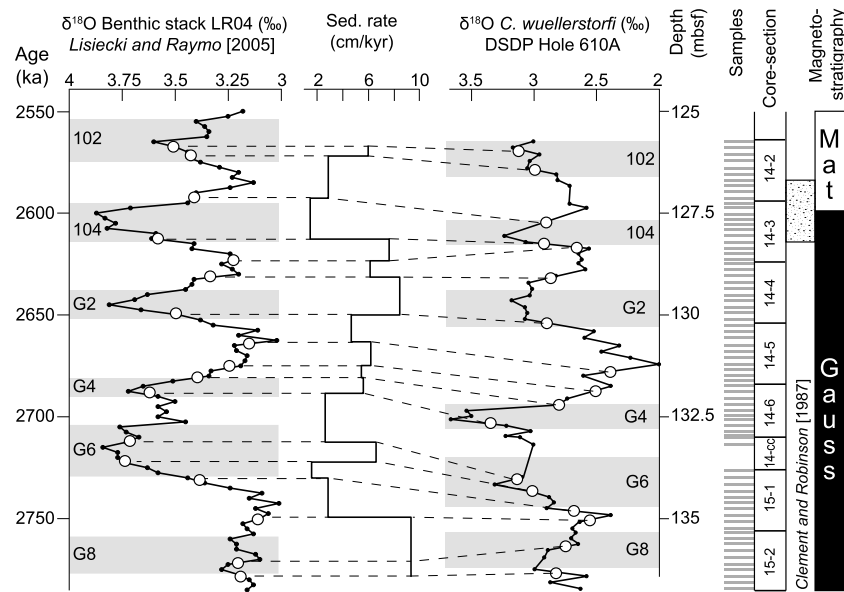
Figure 2. Age model for DSDP Hole 610A based on the graphic correlation of $\delta^{18}O_{benthic}$ to the LR04 benthic stack using Analyseries 2.0.4.2 [*Paillard*, 1996]. Tie points are summarized in Table 1 and the resulting sedimentation rate is displayed in the middle panel. The magnetostratigraphy and its uncertainty interval (stippled) are based on *Clement and Robinson* [1987]. The MIS boundaries and taxonomy follow *Lisiecki and Raymo* [2005].

we used the benthic $\delta^{18}O$-based age model of *Bolton et al.* [2010] for Hole U1313C (Figure 3b). The MIS boundaries in both holes are based on the MIS taxonomy of *Lisiecki and Raymo* [2005].

4.2. Mg/Ca-Derived SST Estimates

For Hole 610A, sea surface temperature estimates range from 7.7°C (2713 ka) to 16.3°C (2780 ka), averaging 13.8°C (Figure 3f). In the lower part of the section, the SST remains around 15°C at the start of MIS G6 (2730 ka) and then drops to the minimum of 7.7°C (2713 ka). During MIS G1, the SST reaches a maximum of 16.0°C (2629 ka) and then falls gradually to a minimum of 11.7°C (2598 ka during MIS 104). In the following interglacial MIS 103, the temperature again rises to 15.7°C (2587 ka).

Table 1. Tie Points Used for the Age Model in DSDP Hole 610A Based On the Graphic Correlation of $\delta^{18}O_{benthic}$ With LR04 Using Analyseries 2.0.4.2 [*Paillard*, 1996]

Depth (mbsf)	Age (ka)
125.93	2567
126.45	2572
127.70	2593
128.28	2613
128.44	2624
129.06	2632
130.21	2651
131.34	2664
131.89	2676
132.26	2682
132.69	2689
134.05	2714
134.31	2724
134.83	2731
135.13	2751
135.71	2771
136.33	2778

In Hole U1313C, SST varies from 11.7°C (2599 ka) to 22.7°C (2750 ka) (Figure 3f). These highest temperatures occur during interglacial G7 after which cooling is evidenced during MIS G6–G4, briefly interrupted near the MIS G5–G4 boundary (21.0°C; 2689 ka). After MIS G4, SST remains high and peaks at 22.6°C (2628 ka) in MIS G1. A severe cooling sets in just prior to MIS 104 including the coldest temperature recorded (11.7°C; 2599 ka) and is followed by a warming during MIS 103 when SSTs remain around 17.5°C until a cooling occurs during MIS 100 (13.2°C; 2532 ka).

4.3. $\delta^{18}O_{bulloides}$ and Relative Salinity

In Hole 610A, $\delta^{18}O_{bulloides}$ remains low (up to ~2‰) until the onset of MIS G6 through MIS G4 when a maximum of 2.55‰ is reached at 2686 ka during MIS G4 (Figure 3c). The $\delta^{18}O_{bulloides}$ record gradually decreases until MIS 104, when it rises again to a maximum of 2.56‰ at 2598 ka followed by a decrease during MIS 103 with a minimum of 1.22‰ at 2583 ka. In Hole U1313C, a peak value (1.85‰) is recorded at 2704 ka followed by a gradual decrease culminating during MIS G2 (0.89‰ at 2652 ka; Figure 3c). The highest values of the interval are recorded during MIS 100 (2.92‰ at 2530 ka).
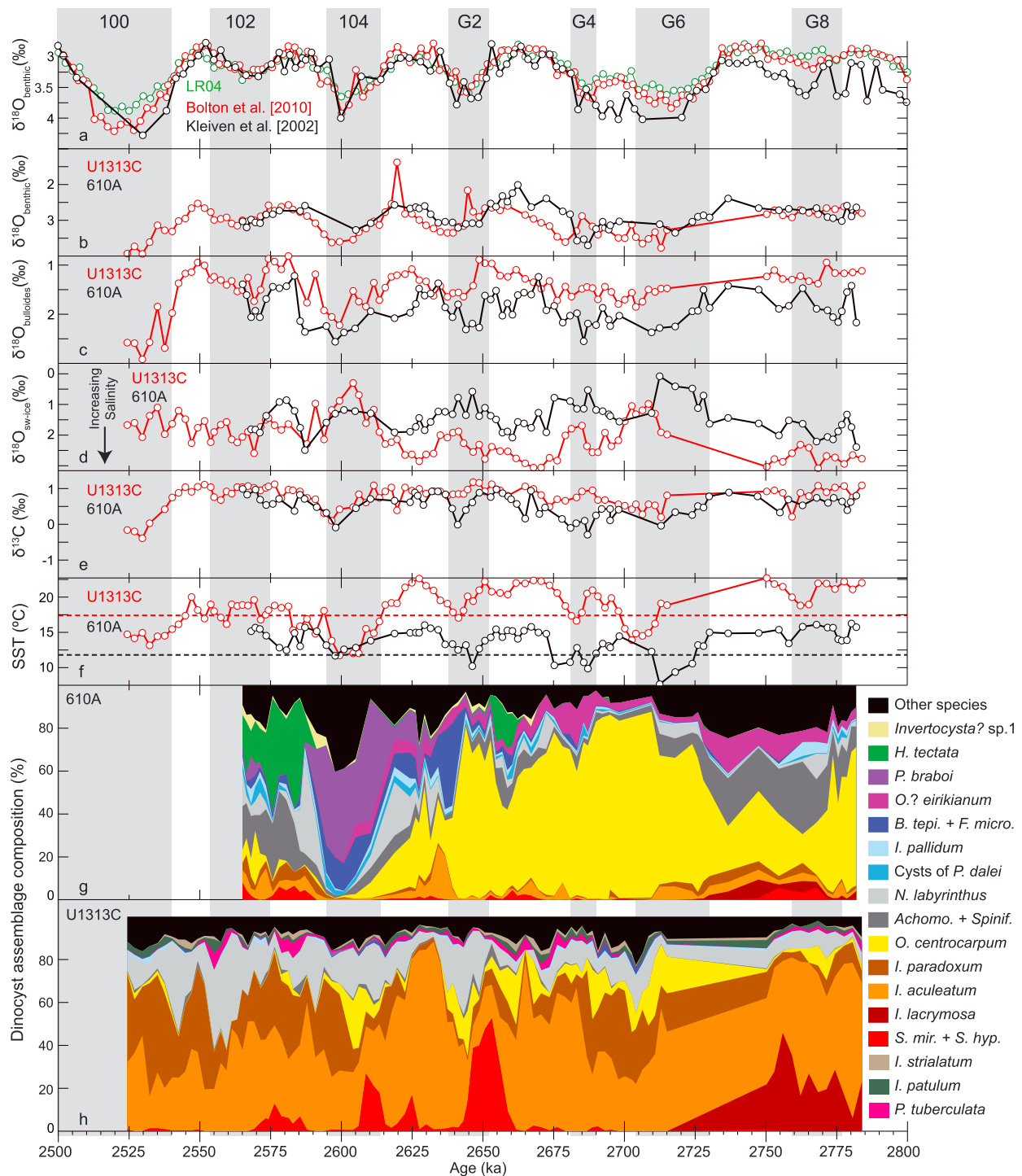
Figure 3. Palynology and foraminiferal geochemistry of the upper Pliocene–lower Pleistocene interval sampled in Holes 610A and U1313C (black and red curves, respectively, in Figures 3b–3f): (a) benthic oxygen isotope records from *Lisiecki and Raymo* [2005] (green), *Bolton et al.* [2010] for Site U1313 (red), and *Kleiven et al.* [2002] for Site 610 (black); (b) benthic oxygen isotope composition; (c) planktonic isotope composition; (d) sea surface salinity estimates based on the planktonic isotope composition; (e) benthic carbon isotope composition; (f) sea surface temperatures based on Mg/Ca of *G. bulloides*; horizontal dashed lines indicate present day sea-surface temperature based on *Locarnini et al.* [2010]; (g) dinoflagellate cyst (dinocyst) assemblage composition in Hole 610A; and (h) dinocyst assemblage composition in Hole U1313C. *H. tectata* = *Habibacysta tectata*; *P. braboi* = *Pyxidinopsis braboi*; *O.?* *eirikianum* = *Operculodinium?* *eirikianum*; *B. tepi.* + *F. micro.* = *Bitectatodinium tepikiense* + *Filisphaera microornata*; *I. pallidum* = *Impagidinium pallidum*; *P. dalei* = *Pentapharsodinium dalei*; *N. labyrinthus* = *Nematosphaeropsis labyrinthus*; *Achomo.* + *Spinif.* = undifferentiated species of *Achomosphaera* and *Spiniferites*; *O. centrocarpum* = *Operculodinium centrocarpum* sensu *Wall and Dale* [1966]; *I. paradoxum* = *Impagidinium paradoxum*; *I. aculeatum* = *Impagidinium aculeatum*; *I. lacrymosa* = *Invertocysta lacrymosa*; *S. mir.* + *S. hyp.* = *Spiniferites mirabilis* + *Spiniferites hyperacanthus*; *I. strialatum* = *Impagidinium strialatum*; *I. patulum* = *Impagidinium patulum*; *P. tuberculata* = *Pyxidinopsis tuberculata*.
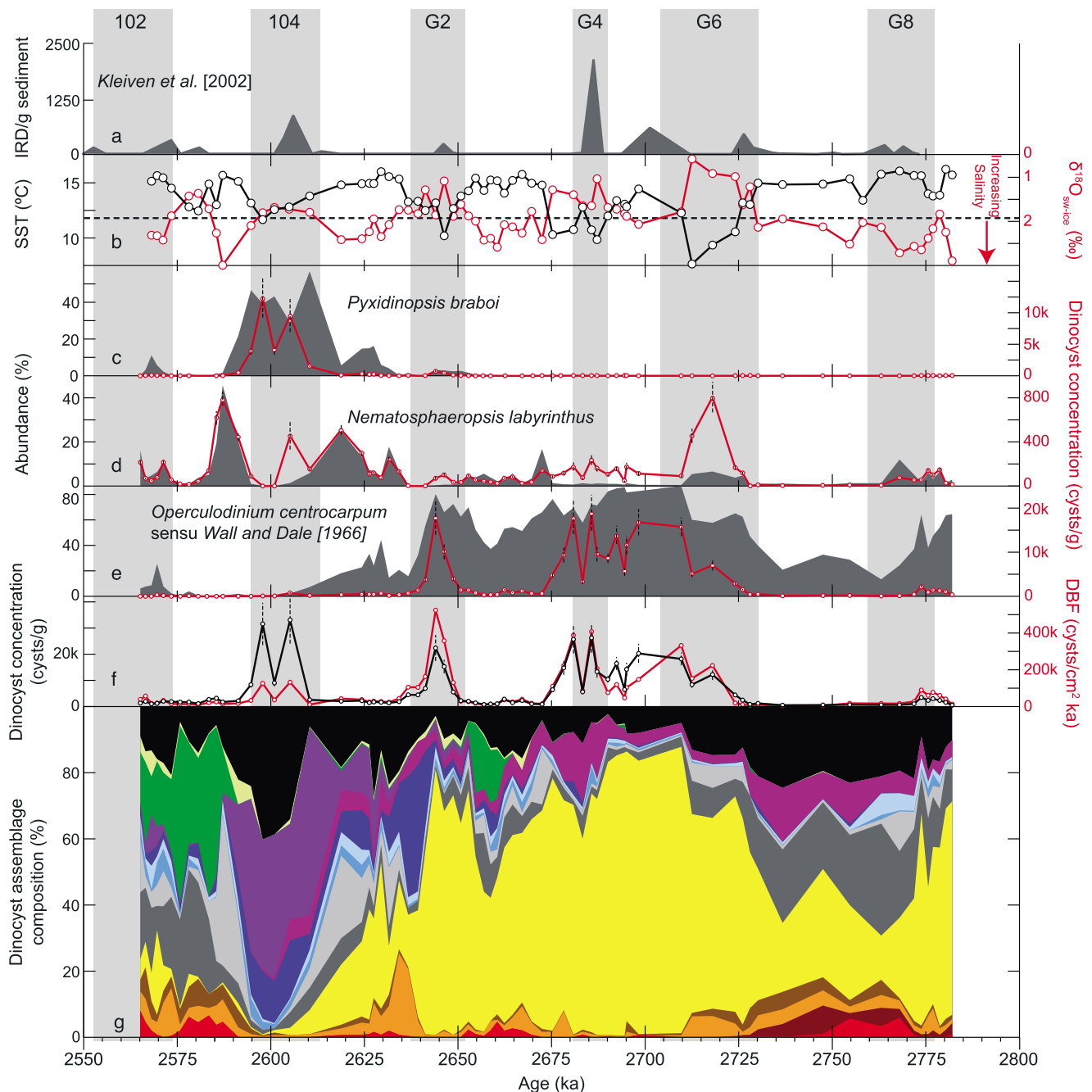
Figure 4. Selected palynology and foraminiferal geochemistry from Site 610: (a) ice-rafted debris record from *Kleiven et al.* [2002]; (b) sea surface temperature and salinity with the present day sea surface temperature as a horizontal dashed line; (c-e) relative abundance and concentration of the dinoflagellate cysts (dinocysts): (c) *Pyxidinopsis braboi*, (d) *Nematosphaeropsis labyrinthus*, and (e) *Operculodinium centrocarpum* sensu *Wall and Dale* [1966]; (f) total dinocyst concentration (black) with error bars following *Stockmarr* [1971] (supporting information) and dinocyst burial flux (red); and (g) dinocyst assemblage composition (see Figure 3 for key).

In Hole 610A, the $\delta^{18}O_{sw-ice}$ record broadly follows the SST curve, with a minimum of −0.03‰ (2713 ka, MIS G6) and a maximum of 2.51‰ (2587, MIS 103). In Hole U1313C, a similar pattern emerges with high relative salinities prior to MIS G6 (3.08‰ at 2768 ka, during MIS G8), a drop during the MIS G6–G4 cold interval (0.98‰ at 2709 ka), and a rise to a maximum in MIS G3 (3.06‰ at 2671 and 2668 ka). A minimum of 0.30‰ is recorded at 2604 ka during MIS 104 followed by relatively stable sea surface salinities fluctuating around 2.0‰.

Figure 5. Selected palynology and foraminiferal geochemistry from Site 607/U1313: (a) quartz to calcite ratio from *Naafs et al.* [2013a]; (b) benthic carbon isotope composition from *Raymo et al.* [1992] for Site 607 (red) and equatorial Pacific Site 677 (green) and from this study for Site U1313 (black). The *Raymo et al.* [1992] age model was reinterpreted by graphic correlation of their $\delta^{18}O_{benthic}$ to the LR04 stack; (c) sea surface temperatures based on Mg/Ca on *G. ruber* from *Friedrich et al.* [2013] (red), alkenone sea surface temperature from *Naafs et al.* [2012], and Mg/Ca on *G. bulloides* from this study (black); (d) relative abundance of *Operculodinium centrocarpum* sensu *Wall and Dale* [1966]; (e) total dinoflagellate cyst (dinocyst) concentration (black) with error bars following *Stockmarr* [1971] (supporting information), and dinoflagellate cyst burial flux (red); and (f) dinocyst assemblage composition (see Figure 3 for key).

4.4. $\delta^{13}C_{benthic}$

In Hole 610A, $\delta^{13}C_{benthic}$ values in the lowest part of the interval remain above 0.5‰ except just before and after MIS G8 (Figure 3e). At the start of the MIS G6–G4 cold period, values drop significantly to a minimum of −0.29‰ at 2687 ka during MIS G4. MIS G3 coincides with a rise to 0.98‰ at 2655 ka. The subsequent interval is characterized by values consistently above 0.5‰ except during glacials when $\delta^{13}C_{benthic}$ reaches minima: −0.01‰ at 2641 ka during MIS G2 and −0.09‰ at 2598 ka during MIS 104.

In Hole U1313C, values around 1.0‰ are recorded prior to MIS G6 followed by a drop to 0.20‰ at 2713 ka (Figure 3e). The following glacials, except for MIS 104, are less well pronounced than in Hole 610A. An absolute minimum of −0.39‰ (2530 ka) is observed during MIS 100.

4.5. Dinoflagellate Cyst Analysis

For Hole 610A, 72 samples (from a total of 73; supporting information) contained sufficient organic material to count at least 300 dinoflagellate cysts (303–806, average 361). Total cyst concentrations range from 505 ± 34 cysts/g (2782 ka) to 33,099 ± 9039 cysts/g (2605 ka; Figure 4f). The error propagation follows the marker grain method of *Stockmarr* [1971], detailed in the supporting information. Cyst concentrations peak during glacials and are lower during interglacials. The DBF has a signature that is comparable to the total concentration, except during MIS 104 when it remains low (Figure 4f). In total, we recognized 82 dinoflagellate cyst taxa with an average of 23 taxa per sample. The most abundant species is *Operculodinium centrocarpum* sensu *Wall and Dale* [1966] (*O. centrocarpum* hereafter) with an average abundance of 40%.

For Hole U1313C, 73 samples (from a total of 94; supporting information) were counted to at least 300 dinoflagellate cysts (302–429, average 372) whereas 21 samples were counted (75–275 cysts, average 167) until two complete slides were scanned. Cyst concentrations range from 15 ± 2 cysts/g (2555 ka) to 1686 ± 161 cysts/g (2527 ka; Figure 5e), an order of magnitude lower than in Hole 610A. The DBF tracks the fluctuations in total concentration closely (Figure 5e). Sixty-one dinoflagellate cyst taxa were described with 16 taxa on average per sample. Assemblages are dominated by *Impagidinium aculeatum* and *Impagidinium paradoxum*, occurring with maximum abundances of 88% (at 2633 ka) and 53% (at 2532 ka), respectively.

5. Discussion

5.1. Salinity and IRD Records

Site 610 is located in the northern part of the IRD belt [*Rasmussen and Thomsen*, 2004], and downhole IRD records document the melting of icebergs since MIS M2 but with an intensification since MIS G4 [*Kleiven et al.*, 2002]. The salinity record from this study shows a reduction in salinity during the glacials when the IRD record reaches maxima (Figures 4a and 4b) and may therefore be related to the influx of fresh water via icebergs. Site U1313 is in the southernmost part of the IRD belt [*Naafs et al.*, 2013a, 2013b]. In Hole U1313C, the quartz/calcite ratio [*Naafs et al.*, 2013a], an indicator for the influx of ice-rafted silicate minerals, records further intensification of NHG during MIS 104 (Figure 5a), which is concurrent with a drop in $\delta^{18}O_{sw-ice}$ (Figure 3d).

5.2. Reworking and Transport in the Palynological Record

The total concentrations of dinoflagellate cysts and their associated DBFs peak in the glacial intervals (Figures 4f and 5e). The 0.6‰ $\delta^{18}O_{benthic}$ increase provides evidence of a eustatic drop of about 45 m [*Bintanja and Van de Wal*, 2008] between MIS G8 and G4. Combined with the appearance of IRD [*Kleiven et al.*, 2002; *Naafs et al.*, 2013a], it could be argued that the peaks in dinoflagellate cyst concentration and DBF contain a transported/reworked component from the episodically exposed shelf. However, the palynological record itself bears evidence of only limited coastal reworking and transport: (1) Peak glacial assemblages do not contain prominent abundances of species commonly found in the coastal environments of temperate regions [*Wall et al.*, 1977; *Zonneveld et al.*, 2013]; (2) cysts of heterotrophic dinoflagellates, which are abundant in coastal temperate and polar regions today [*Wall et al.*, 1977; *Zonneveld et al.*, 2013], are poorly represented; (3) the dinoflagellate cyst to pollen ratio fluctuates between 0.97 and 0.99 in both holes, indicating a very limited inner shelf influence [*Versteegh and Zonneveld*, 1994]; and (4) identifiably reworked marine palynomorphs were present in very low abundances: a maximum reworking rate of 3% in Hole 610A and 2% in Hole U1313C.

Versteegh et al. [1996] already noted increasing dinoflagellate cyst concentrations during cooler phases in Hole 607, of which U1313C is a re-drill. These authors proposed that changes in ocean circulation, possibly

induced by changing atmospheric circulation, led to the introduction of nutrient-rich waters to Site 607/U1313C during these colder phases thereby resulting in enhanced productivity. Our data from Hole U1313C also show increases in dinoflagellate cyst concentration and DBF during glacials (Figure 5e). A similar pattern is seen for the glacial stages in Hole 610A, except for MIS 104 where concentration peaks but DBF (a better measure of productivity) barely surpass interglacial values (Figure 4f). This suggests that during MIS 104 at Site 610, productivity was much lower than during the preceding glacials, presumably reflecting lower nutrient levels.

5.3. Mg/Ca SST

The SST records capture the glacial–interglacial variations well in the observed time slab and the glacial coolings are coeval at both sites, except for the sustained cold period G6–G4 where the coolest interval in U1313C seems to lag the coolest period in 610A. During MIS 104, SSTs in Hole U1313C drop close to values recorded for Hole 610A showing a disappearance of the meridional SST gradient. The U1313 SST record from the current study compares well to paleotemperature records based on alkenones [*Naafs et al.*, 2012] although values are somewhat lower than those based on the Mg/Ca ratio of *G. ruber* [*Friedrich et al.*, 2013] from the same site (Figure 5c). For Site 607/U1313, *Robinson et al.* [2008] showed that Mg/Ca-derived SST estimates on *G. ruber* are 5.4°C higher than the estimates based on *G. bulloides*. These authors attribute the difference to the fact that *G. bulloides* records early spring SST whereas *G. ruber* compares well to faunal-based SST estimates for August.

5.4. Paleoceanographic History

The combined palynological and geochemical signals of both holes reveal a detailed history of events leading toward and across the Neogene–Quaternary (Pliocene–Pleistocene) climatic transition in the eastern North Atlantic. In the following discussion, we utilize variations in the abundance of *O. centrocarpum* to track the NAC throughout this crucial interval. In modern North Atlantic sediments, high abundances of this species are associated with the presence of the NAC [e.g., *Harland*, 1983; *Rochon et al.*, 1999]. During the glacial MIS M2 (circa 3.3 Ma), a sudden decline in its relative abundance has been linked to a southward shift of the NAC which halted the transport of warm waters to high latitudes and induced an expansion of continental ice sheets [*De Schepper et al.*, 2009, 2013].

5.4.1. MIS G9 to Onset of MIS G6

In both holes, the interval leading up to MIS G6 is characterized by limited global ice volume (low $\delta^{18}O_{benthic}$), a low influx of IRD [*Kleiven et al.*, 2002; *Naafs et al.*, 2013a], and a high influence of NADW (high $\delta^{13}C_{benthic}$) [*Raymo et al.* 1992; *Ravelo and Andreasen*, 2000; *Ravelo and Hillaire-Marcel*, 2007] reflecting a vigorous Atlantic THC. In Hole 610A, a decline in *O. centrocarpum* is noticeable during MIS G8, but abundance never drops below 20%. Combined with stable, high relative salinity ($\delta^{18}O_{sw-ice}$ 2.5–2.0‰) and SST (14–16°C) estimates, we infer an active NAC over Site 610.

In Hole U1313C, *I. aculeatum* and *I. lacrymosa* dominate assemblages. *Impagidinium aculeatum* is associated with warm, oligotrophic water masses in modern [*Zonneveld et al.*, 2013] and Pliocene sediments [*De Schepper et al.*, 2011], reflecting open-ocean conditions with a limited influence of the NAC. *Invertocysta lacrymosa*, linked also to warm water masses [*Versteegh and Zonneveld*, 1994; *De Schepper et al.*, 2011], disappears from the record in both holes (Figures 3g and 3h). Its disappearance from central and eastern North Atlantic Sites U1313 (2715 ka) and 610 (2724 ka) in this study and all other North Atlantic sites [*Harland*, 1979; *de Vernal and Mudie*, 1989; *Versteegh*, 1997; *De Schepper et al.*, 2009] presumably reflects significant cooling leading to MIS G6 [*De Schepper and Head*, 2008].

5.4.2. MIS G6–G1: Dominance of *O. centrocarpum* in Hole 610A

During the MIS G6–G4 glacial interval, the $\delta^{13}C_{benthic}$ signature of both holes suggests an increased influence of AABW. The palynological record of Hole 610A is dominated by *O. centrocarpum* (up to 87% at 2710 ka) during MIS G6, a result of the strong influence of the NAC over Site 610 even throughout this glacial interval.

Across the MIS G3/G2 transition, concurrent with increasing $\delta^{18}O_{benthic}$ and $\delta^{18}O_{bulloides}$ and a SST of 21°C, a distinct abundance peak of *Spiniferites mirabilis* (53%) is recorded in Hole U1313C. This species is regarded as an indicator of warm water masses in an open-ocean setting [*Zonneveld et al.*, 2013]. Based on its modern distribution, with high abundances mostly in the eastern Atlantic Ocean [*Harland*, 1983; *Rochon et al.*, 1999],

Versteegh [1997] hypothesized that the increased abundance at Site 607/U1313 during the Pliocene was caused by an influx of surface waters from the east, consistent with modern circulation patterns (Figure 1).

In Hole 610A, the cool water indicator *Habibacysta tectata* [*Head et al.*, 1989; *Head*, 1994; *Versteegh*, 1994, 1997] appears at the end of interglacial MIS G3 (Figure 3g). It is rapidly replaced by *O. centrocarpum* which peaks shortly after *S. mirabilis* in U1313C indicating NAC influence over Hole 610A and warm open-ocean conditions over U1313C across the MIS G3–G2 boundary. However, at the end of glacial MIS G2, the cool-tolerant species *Bitectatodinium tepikiense* and *Filisphaera microornata* replace *O. centrocarpum* in Hole 610A (Figure 4g). The affinity of *B. tepikiense* for cool water masses might be related to enhanced water stratification [*Rochon et al.*, 1999; *de Vernal et al.*, 2005; *de Vernal and Marret*, 2007] which would then provide evidence for a reduced influence of the NAC close to Site 610. In Hole U1313C, maxima in SST and $\delta^{18}O_{sw-ice}$ combined with the absolute dominance of *I. aculeatum* suggest warm, oligotrophic, conditions in the North Atlantic subtropical gyre.

5.4.3. MIS G1–102

In the latter half of MIS G1 in Hole 610A, *O. centrocarpum* is replaced by *Nematosphaeropsis labyrinthus* (Figures 4c and 4d), a species tolerant of high-amplitude changes in salinity and SST [*Zonneveld et al.*, 2013] and indicative of rapidly changing oceanic conditions in the Pleistocene North Atlantic [*Baumann and Matthiessen*, 1992; *Eynaud et al.*, 2004; *Penaud et al.*, 2008]. Glacial MIS 104 is characterised by an acme of *Pyxidinopsis braboi* (up to 57% at 2610 ka). This enigmatic species was described from the Pliocene of Belgium [*De Schepper et al.*, 2004] and since reported only from the Plio-Pleistocene of Hole 610A [*De Schepper and Head*, 2009] and the Miocene of the Antarctic Ross Sea where it was considered a pioneering species able to survive extended intervals of ice cover [*Warny et al.*, 2009]. Therefore, the replacement of *O. centrocarpum* first by *N. labyrinthus* and then by *P. braboi* signifies a shift from NAC conditions via a transitional, highly variable hydrography to a polar-influenced environment. Interestingly, the disappearance of the NAC at Site 610A around 2.6 Ma corresponds to the arrival in the eastern North Atlantic of IRD sourced from a North American ice sheet [*Bailey et al.*, 2013] which also episodically influenced the dust flux in Hole U1313C since 2.7 Ma [*Naafs et al.*, 2012]. Around the same time, *Thierens et al.* [2013] hypothesized the presence of ice sheets on the British Isles. These observations are in line with the proxy records from the current study showing that the Arctic Front, which had been progressively shifting southward from the Norwegian Sea toward the North Atlantic since 3.0 Ma [*Henrich et al.*, 2002], must have been close to Site 610 during MIS 104. Following the acme of *P. braboi* are high abundances of *N. labyrinthus* concurrent with large fluctuations in $\delta^{18}O_{bulloides}$ and relative salinity, and modest SST fluctuations (Figures 3 and 4).

In Hole U1313C, the geochemical proxies show a typical glacial signature during MIS 104, with SST lower than any of the preceding glacial values in the sampled interval, a high concentration of dinoflagellate cysts, also documented by *Versteegh*. [1997], and increased presence of ice-rafted debris [*Naafs et al.*, 2013a] (Figure 5a). The meridional SST gradient, apparent throughout the entire sampled interval up to MIS 104, disappears completely. Similarly, the glacial $\delta^{13}C$ values during MIS 104 from both studied sites are comparable, which has no precedent in any of the glacials from the studied time slab and points to a reduced influence of NADW and hence reduction in North Atlantic THC. The dinoflagellate cyst assemblages in Hole U1313C record a decline in *I. aculeatum* and a peak in *O. centrocarpum* coeval with the acme of *P. braboi* in Hole 610A (Figure 5d). We interpret this as a southward shift of the NAC, a scenario described for the North Atlantic in census studies of planktonic foraminifers for the Last Glacial Maximum [*Pflaumann et al.*, 2003] and in proxy studies for mid-Pleistocene glacial stages [*Alonso-Garcia et al.*, 2011], the late Pliocene [*Naafs et al.*, 2010], and MIS M2 during the Piacenzian [*De Schepper et al.*, 2009, 2013].

5.4.4. MIS 101–MIS 100 in Hole U1313C

From this interval, we have data only from Hole U1313C, with low interglacial values for the oxygen isotope records from both planktonic and benthic foraminifers. Salinity continued to fluctuate moderately and the high $\delta^{13}C$ values show a clear influence of NADW. At the start of MIS 100; however, a clear increase in $\delta^{18}O_{benthic}$ and $\delta^{18}O_{benthic}$ coincides with a decrease in SST, showing the extensive growth of continental ice sheets during MIS 100 [*Raymo et al.*, 1989; *Raymo and Ruddiman*, 1992] with IRD discharge in the IRD belt [*Kleiven et al.*, 2002; *Naafs et al.*, 2013a]. Marine isotope stage 100 is seen as the first intense glacial controlled mainly by obliquity forcing [*Shackleton et al.*, 1984]. The $\delta^{13}C$ estimates of this study compare well to previous estimates based on *Cibicidoides* spp. at the same site and are higher than estimates for Hole 677 in the equatorial Pacific Ocean [*Raymo et al.*, 1992] (Figure 5b).

5.5. Implications for iNHG

Our palynological evidence from Hole 610A reveals a persistent NAC until MIS 104 (2.60 Ma), about 140 kyr after the well-documented cooling and appearance of circum-Atlantic ice sheets around 2.7 Ma [*Naafs et al.,* 2012, 2013a; *Bailey et al.,* 2013] near the MIS G7–G6 boundary (2.74 Ma). This result suggests that an influence other than an active NAC is crucial in controlling high-latitude temperatures, possibly pCO_2 as advanced by *Lunt et al.* [2008a, 2008b], *Pagani et al.* [2010], *Seki et al.* [2010], and *Bartoli et al.* [2011]. Moreover, using modeling studies, *Lunt et al.* [2008a, 2008b] convincingly showed that a persistent NAC was not likely a pivotal factor in the expansion of Northern Hemisphere ice sheets. *Kleiven et al.* [2002] proposed a progressive circum-Atlantic glaciation between 3.5 and 2.4 Ma. *Bailey et al.* [2013] showed that the North American ice sheets reached the coastline around 2.64 Ma, only from then onward contributing to IRD in the North Atlantic, while ice sheets on the British Isles were a source of IRD since 2.60 Ma [*Thierens et al.,* 2013]. These events may well be linked to the reduced high-latitude influence of the NAC at Site 610 starting at 2.64 Ma, and its disappearance around 2.60 Ma concurrent with the collapse in meridional SST gradient documented in this study. It appears that during MIS 104, the Northern Hemisphere switched to a profound glacial state in which polar influences extended to the midlatitudes of the North Atlantic Ocean.

5.5.1. Southward Shift of the Arctic Front and NAC

Recently, *Friedrich et al.* [2013] argued against significant southward movement of the NAC during iNHG based on Mg/Ca analyses on *G. ruber* from Site U1313. Our suite of palynological and geochemical proxies from Holes 610A and U1313C contradicts those findings. Three lines of evidence reveal a southward shift of the Arctic Front to a position close to Site 610 and of the NAC to a position close to Site U1313 around iNHG.

First, the NAC indicator *O. centrocarpum* disappears from the Hole 610A assemblages during MIS 104 and is replaced by the cold tolerant *P. braboi* (Figure 4) while a concurrent peak in *O. centrocarpum* abundance appears in the U1313C record. Additionally, some specimens of *P. braboi* have been retrieved from Hole U1313C, coeval with its acme documented in Hole 610A, corroborating the evidence for a widespread cooling in the North Atlantic and a southern shift of cold-tolerant species.

Second, the collapse of the meridional SST gradient, apparent during MIS 104 (Figure 3f) is one of two requirements for a southward shift of strong westerlies [*Budikova,* 2009]. The second requirement is an increased geopotential height over the high latitudes, which has been shown to occur in the extant Arctic Ocean during episodes with extensive sea ice formation [*Jaiser et al.,* 2012]. We hypothesize a similar effect on the high-latitude atmosphere with a southward shift of the westerlies caused by the expansion of the circum-Atlantic ice sheets. The driving mechanism of the NAC has both thermohaline and wind stress components [e.g., *Hansen and Østerhus,* 2000], and a change in Northern Hemisphere atmospheric circulation is therefore likely to affect the position of the NAC. For the late Pliocene–early Pleistocene interval, a similar scenario, in which changes in atmospheric circulation induce changes in NAC position, has already been proposed [*Versteegh et al.,* 1996; *Naafs et al.,* 2010]. When taking these observations together, we propose that atmospheric circulation altered significantly near the Pliocene–Pleistocene boundary.

Third, the difference between DBF and dinocyst concentration in MIS 104 suggests a fundamental change in water mass composition over Site 610 in comparison to the preceding glacials (see section 5.2). *Versteegh et al.* [1996] showed that the unexpected high dinoflagellate cyst concentrations during glacials can be attributed to higher nutrient influx. Our DBF values support this for all glacials in both holes, except for MIS 104 in 610A where the DBF is more comparable to interglacial values. This might signal lower levels of nutrients in the surface waters than during preceding glacials as a result of the more southerly position of the NAC.

5.5.2. The Base of the Quaternary and Climatic Reorganization of the Northern Hemisphere

The southward shift of the NAC during MIS 104 accompanied simultaneous cooling in northwestern Europe, as evidenced by the transition from the Reuverian to Praetiglian pollen stages in the Netherlands [*Zagwijn,* 1985] and southern Europe as seen also from the pollen record [*Suc and Zagwijn,* 1983]. In the North Sea, cooling is expressed not only by the pollen record but also through changes in the dinoflagellate cyst assemblages, including the earliest acme of *Filisphaera/Habibacysta/Bitectatodinium* [*Kuhlmann et al.,* 2006a, 2006b] which is comparable to the MIS 104–102 record of Hole 610A in the present study. In eastern England, the disappearance of thermophilic dinoflagellate cyst species near the base of the Quaternary [*Head,* 1998] may similarly reflect this climate shift although independent age control is poor.

A similar atmospheric reorganization to that hypothesized here was proposed for the sudden strengthening of the winter monsoon over the Chinese loess plateau [*An et al.*, 1991; *Liu and Ding*, 1998]. A high-pressure system became active over Siberia and Mongolia as a result of an increase in global ice volume and ice-covered area [*Ding et al.*, 1995]. This led to a significant weakening of summer monsoon strength at 2.6 Ma, as inferred from a southward expansion of the deserts in northern China [*Ding et al.*, 2005]. Coupled atmosphere-ocean modeling experiments show that the suppression of the Asian summer monsoon is linked to a cooler North Atlantic Ocean and a weakened THC [*Lu and Dong*, 2008]. The current study offers proxy data in support of this suggestion with a cooling of the North Atlantic and the collapse of the meridional SST gradient during MIS 104.

The lowering of the base of the Quaternary System and Pleistocene Series from 1.8 Ma to 2.58 Ma utilized an existing global boundary stratotype section and point (GSSP) at Monte San Nicola, in Sicily [*Gibbard and Head*, 2010; *Gibbard et al.*, 2010]. This GSSP is just 1 m above the Gauss–Matuyama paleomagnetic reversal, not only facilitating global correlation but also representing a convenient midpoint in a series of profound global cooling events between 2.8 and 2.4 Ma including several events considered to correspond closely to the new boundary [*Head et al.*, 2008]. *Bailey et al.* [2013] have already noted that the new base of the Quaternary may be closely associated temporally with the first major glaciation of North America, and *Thierens et al.* [2013] demonstrate midlatitude ice sheet development on the British Isles and Ireland around 2.6 Ma. Our present study suggests that the base of the Quaternary coincides closely with a major climatic reorganization of the Northern Hemisphere in line with these previous observations.

6. Conclusions

We sampled a 260 kyr time slab (MIS G9–100; circa 2.78–2.52 Ma) straddling the base of the Quaternary (2.58 Ma) from DSDP Hole 610A, today in the path of the NAC, and IODP Hole U1313C, in the extant North Atlantic subtropical gyre. Dinoflagellate cyst assemblages were combined with benthic and planktonic foraminiferal geochemistry to document paleoceanographic changes in this climatically important interval. At around 2.74 Ma during MIS G6, our geochemical records show a shift to cooler conditions and fresher water masses in both studied holes. Aside from the highest occurrence of *I. lacrymosa* (2.72 Ma in 610A; 2.74 Ma in U1313C), which is shown to be a good stratigraphic marker at these latitudes, no major cooling is recorded in the dinoflagellate cyst assemblage composition at this time. There follows a ~140 kyr interval characterized by the dominance of *O. centrocarpum* sensu *Wall and Dale* [1966], most notably over Site 610, which indicates an active NAC at the time.

After the dominance of *O. centrocarpum*, a striking assemblage turnover occurs during MIS 104, with a sudden peak in the cold tolerant *P. braboi* in Hole 610A indicating close proximity to the Arctic front at 2.61 Ma. The southward deflection of the NAC is indicated by a peak in *O. centrocarpum* over Site U1313 at the inception of MIS 104. At this point, we hypothesize that elevated atmospheric pressure over the Arctic, brought about by the expanding circum-Atlantic ice sheets, caused the NAC to shift southward during MIS 104. The abrupt cooling in the North Sea and northwestern Europe, the widespread deposition of loess-paleosol sequences over China, and the expansion of deserts over northern Asia all appear causally linked to this final step in the glaciation of the Northern Hemisphere.

References

Alonso-Garcia, M., F. J. Sierro, and J. A. Flores (2011), Arctic front shifts in the subpolar North Atlantic during the mid-Pleistocene (800–400 ka) and their implications for ocean circulation, *Palaeogeogr. Palaeoclimatol. Palaeoecol.*, *311*, 268–280, doi:10.1016/j.palaeo.2011.09.004.

An, Z., G. Kukla, S. C. Porter, and J. Xiao (1991), Late Quaternary dust flow on the Chinese loess plateau, *Catena*, *18*(2), 125–132, doi:10.1016/0341-8162(91)90012-M.

Bacon, S. (1997), Circulation and fluxes in the North Atlantic between Greenland and Ireland, *J. Phys. Oceanogr.*, *27*(7), 1420–1435, doi:10.1175/1520-0485(1997)027 < 1420:CAFITN > 2.0.CO;2.

Bailey, I., G. M. Hole, G. L. Foster, P. A. Wilson, C. D. Storey, C. N. Trueman, and M. E. Raymo (2013), An alternative suggestion for the Pliocene onset of major Northern Hemisphere glaciation based on the geochemical provenance of North Atlantic Ocean ice-rafted debris, *Quat. Sci. Rev.*, *75*(1), 181–194, doi:10.1016/j.quascirev.2013.06.004.

Barker, S., M. Greaves, and H. Elderfield (2003), A study of cleaning procedures used for foraminiferal Mg/Ca paleothermometry, *Geochem. Geophys. Geosyst.*, *4*(9), 8407, doi:10.1029/2003GC000559.

Bartoli, G., M. Sarnthein, M. Weinelt, H. Erlenkeuser, D. Garbe-Schönberg, and D. W. Lea (2005), Final closure of Panama and the onset of Northern Hemisphere glaciation, *Earth Planet. Sci. Lett.*, *237*, 33–44, doi:10.1016/j.epsl.2005.06.020.

Bartoli, G., B. Hoenisch, and R. E. Zeebe (2011), Atmospheric CO₂ decline during the Pliocene intensification of Northern Hemisphere glaciations, *Paleoceanography*, *26*, PA4213, doi:10.1029/2010PA002055.

Baumann, K., and J. Matthiessen (1992), Variations in surface water mass conditions in the Norwegian Sea: Evidence from Holocene coccolith and dinoflagellate cyst assemblages, *Mar. Micropaleontol.*, 20(2), 129–146, doi:10.1016/0377-8398(92)90003-3.

Bé, A. (1980), Gametogenic calcification in a spinose planktonic foraminifer, *Globigerinoides sacculifer* (Brady), *Mar. Micropaleontol.*, 5, 283–310, doi:10.1016/0377-8398(80)90014-6.

Bintanja, R., and R. S. W. van de Wal (2008), North American ice-sheet dynamics and the onset of 100,000-year glacial cycles, *Nature*, 454(7206), 869–872, doi:10.1038/nature07158.

Bolton, C. T., P. A. Wilson, I. Bailey, O. Friedrich, C. J. Beer, J. Becker, S. Baranwal, and R. Schiebel (2010), Millennial-scale climate variability in the subpolar North Atlantic Ocean during the late Pliocene, *Paleoceanography*, 25, PA4218, doi:10.1029/2010PA001951.

Budikova, D. (2009), Role of Arctic sea ice in global atmospheric circulation: A review, *Global Planet. Change*, 68(3), 149–163, doi:10.1016/j.gloplacha.2009.04.001.

Cane, M. A., and P. Molnar (2001), Closing of the Indonesian seaway as a precursor to east African aridification around 3–4 million years ago, *Nature*, 411(6834), 157–162, doi:10.1038/35075500.

Clement, B. M., and F. Robinson (1987), The magnetostratigraphy of Leg 94 sediments, *Proc. Deep Sea Drill. Project Init. Rep.*, 94, 1–16.

Coplen, T. B. (1995), New IUPAC guidelines for the reporting of stable hydrogen, carbon, and oxygen isotope-ratio data, *J. Res. Nat. Inst. Stand. Technol.*, 100, 285.

Cronin, T. (1991), Pliocene shallow-water paleoceanography of the North-Atlantic Ocean based on marine ostracodes, *Quat. Sci. Rev.*, 10, 175–188, doi:10.1016/0277-3791(91)90017-o.

Curry, W. B., and D. W. Oppo (2005), Glacial water mass geometry and the distribution of δ^{13}C of ΣCO_2 in the western Atlantic Ocean, *Paleoceanography*, 20, PA1017, doi:10.1029/2004PA001021.

Curry, W. B., J.-C. Duplessy, L. D. Labeyrie, and N. J. Shackleton (1988), Changes in the distribution of δ^{13}C of deep water ΣCO_2 between the Last Glaciation and the Holocene, *Paleoceanography*, 3(3), 317–341, doi:10.1029/PA003i003p00317.

De Schepper, S., J. Groeneveld, B. D. A. Naafs, C. Van Renterghem, J. Hennissen, M. J. Head, S. Louwye, and K. Fabian (2013), Northern Hemisphere Glaciation during the globally warm early late Pliocene, *PLoS ONE*, 8(12), e81508, doi:10.1371/journal.pone.0081508.

De Schepper, S., and M. J. Head (2008), Age calibration of dinoflagellate cyst and acritarch events in the Pliocene–Pleistocene of the eastern North Atlantic (DSDP Hole 610A), *Stratigraphy*, 5(2), 137–161.

De Schepper, S., and M. J. Head (2009), Pliocene and Pleistocene dinoflagellate cyst and acritarch zonation of DSDP Hole 610A, eastern North Atlantic, *Palynology*, 33(1), 179–218, doi:10.2113/gspalynol.33.1.179.

De Schepper, S., M. J. Head, and S. Louwye (2004), New dinoflagellate cyst and incertae sedis taxa from the Pliocene of northern Belgium, southern North Sea Basin, *J. Paleontol.*, 78(4), 625–644.

De Schepper, S., M. J. Head, and J. Groeneveld (2009), North Atlantic Current variability through marine isotope stage M2 (circa 3.3 Ma) during the mid-Pliocene, *Paleoceanography*, 24, PA4206, doi:10.1029/2008PA001725.

De Schepper, S., E. I. Fischer, J. Groeneveld, M. J. Head, and J. Matthiessen (2011), Deciphering the palaeoecology of late Pliocene and early Pleistocene dinoflagellate cysts, *Palaeogeogr. Palaeoclimatol. Palaeoecol.*, 309, 17–32, doi:10.1016/j.palaeo.2011.04.020.

de Vernal, A., and F. Marret (2007), Organic-walled dinoflagellate cysts: Tracers of sea-surface conditions, in *Proxies in Late Cenozoic Paleoceanography*, vol. 1, edited by C. Hillaire-Marcel and A. de Vernal, pp. 371–408, Elsevier, Rotterdam, doi:10.1016/S1572-5480(07)01014-7.

de Vernal, A., and P. J. Mudie (1989), Pliocene and Pleistocene palynostratigraphy at ODP Sites 646 and 647, eastern and southern Labrador Sea, *Proc. Ocean Drill. Program Sci. Res.*, 105, 401–422, doi:10.2973/odp.proc.sr.105.134.1989.

de Vernal, A., et al. (2005), Reconstruction of sea-surface conditions at middle to high latitudes of the Northern Hemisphere during the Last Glacial Maximum (LGM) based on dinoflagellate cyst assemblages, *Quat. Sci. Rev.*, 24(7–9), 897–924, doi:10.1016/j.quascirev.2004.06.014.

Ding, Z., T. Liu, N. W. Rutter, Z. Yu, Z. Guo, and R. Zhu (1995), Ice-volume forcing of East Asian winter monsoon variations in the past 800,000 years, *Quat. Res.*, 44(2), 149–159, doi:10.1006/qres.1995.1059.

Ding, Z. L., E. Derbyshire, S. L. Yang, J. M. Sun, and T. S. Liu (2005), Stepwise expansion of desert environment across northern China in the past 3.5 Ma and implications for monsoon evolution, *Earth Planet. Sci. Lett.*, 237(1), 45–55, doi:10.1016/j.epsl.2005.06.036.

Dowsett, H. J., and R. Poore (1991), Pliocene sea-surface temperatures of the North Atlantic Ocean at 3.0 Ma, *Quat. Sci. Rev.*, 10, 189–204, doi:10.1016/0277-3791(91)90018-P.

Dowsett, H. J., M. A. Chandler, and M. M. Robinson (2009), Surface temperatures of the Mid-Pliocene North Atlantic Ocean: implications for future climate, *Phil. T. R. Soc. A*, 367(1886), 69–84, doi:10.1098/rsta.2008.0213.

Dowling, L., and I. N. McCave (1993), Sedimentation on the Feni Drift and Late Glacial bottom water production in the northern Rockall Trough, *Sediment. Geol.*, 82, 79–87, doi:10.1016/0037-0738(93)90114-K.

Driscoll, N. W., and G. H. Haug (1998), A short circuit in thermohaline circulation: A cause for Northern Hemisphere glaciation?, *Science*, 282(5388), 436–438, doi:10.1126/science.282.5388.436.

Elderfield, H., and G. Ganssen (2000), Past temperature and δ^{18}O of surface ocean waters inferred from foraminiferal Mg/Ca ratios, *Nature*, 405, 442–445, doi:10.1038/35013033.

Expedition 306 Scientists (2006), Site U1313, *Proc. Integr. Ocean Drill Program*, 303/306, 1–124, doi:10.2204/iodp.proc.303306.112.2006.

Eynaud, F., J. L. Turon, and J. Duprat (2004), Comparison of the Holocene and Eemian palaeoenvironments in the South Icelandic Basin: Dinoflagellate cysts as proxies for the North Atlantic surface circulation, *Rev. Palaeobot. Palynol.*, 128(1–2), 55–79, doi:10.1016/S0034-6667(03)00112-X.

Friedrich, O., P. A. Wilson, C. T. Bolton, C. J. Beer, and R. Schiebel (2013), Late Pliocene to early Pleistocene changes in the North Atlantic Current and suborbital-scale sea-surface temperature variability, *Paleoceanography*, 28, 274–282, doi:10.1002/palo.20029.

Ganachaud, A., and C. Wunsch (2000), Improved estimates of global ocean circulation, heat transport and mixing, from hydrographic data, *Nature*, 408(6811), 453–457, doi:10.1038/35044048.

Gibbard, P. L., and M. J. Head (2010), The newly-ratified definition of the Quaternary System/Period and redefinition of the Pleistocene Series/Epoch, and comparison of proposals advanced prior to formal ratification, *Episodes*, 33, 152–158.

Gibbard, P. L., M. J. Head, M. J. C. Walker, and The Subcommission on Quaternary Stratigraphy (2010), Formal ratification of the Quaternary System/Period and the Pleistocene Series/Epoch with a base at 2.58 Ma, *J. Quat. Sci.*, 25(2), 96–102, doi:10.1002/jqs.1338.

Hansen, B., and S. Østerhus (2000), North Atlantic–Nordic Seas exchanges, *Prog. Oceanogr.*, 45, 109–208, doi:10.1016/S0079-6611(99)00052-X.

Harland, R. (1979), Dinoflagellate biostratigraphy of Neogene and Quaternary sediments at Holes 400/400a in the Bay of Biscay (Deep Sea Drilling Project Leg 48), *Proc. Deep Sea Drill. Project Init. Rep.*, 48, 531–545, doi:10.2973/dsdp.proc.48.122.1979.

Harland, R. (1983), Distribution maps of recent dinoflagellate cysts in bottom sediments from the North Atlantic Ocean and adjacent seas, *Palaeontology*, 26, 321–387.

Haywood, A. M., H. J. Dowsett, P. J. Valdes, D. J. Lunt, J. E. Francis, and B. W. Sellwood (2009), Introduction. Pliocene climate, processes and problems, *Phil. T. R. S. A*, 367(1886), 3–17, doi:10.1098/rsta.2008.0205.

Haug, G. H., and R. Tiedemann (1998), Effect of the formation of the Isthmus of Panama on Atlantic Ocean thermohaline circulation, *Nature*, *393*(6686), 673–676, doi:10.1038/31447.

Haug, G. H., D. Sigman, R. Tiedemann, T. Pedersen, and M. Sarnthein (1999), Onset of permanent stratification in the subarctic Pacific Ocean, *Nature*, *401*(6755), 779–782, doi:10.1038/44550.

Head, M. J. (1994), Morphology and paleoenvironmental significance of the Cenozoic dinoflagellate genera *Tectatodinium* and *Habibacysta*, *Micropaleontology*, *40*(4), 289–321.

Head, M. J. (1998), Marine environmental change in the Pliocene and early Pleistocene of eastern England: The dinoflagellate evidence reviewed, *Meded. Nederlands Inst. Toegepaste Geowetenschappen TNO*, *60*, 199–225.

Head, M. J., G. Norris, and P. J. Mudie (1989), Palynology and dinocyst stratigraphy of the upper Miocene and lowermost Pliocene, ODP Leg 105, Site 646, Labrador Sea, *Proc. Ocean Drill. Program Sci. Res.*, *105*, 423–451, doi:10.2973/odp.proc.sr.105.135.1989.

Head, M. J., P. L. Gibbard, and A. Salvador (2008), The Quaternary: Its character and definition, *Episodes*, *31*(2), 234–238.

Hennissen, J. A. I. (2013), Late Pliocene–early Pleistocene North Atlantic circulation: Integrating dinocyst assemblages and foraminiferal geochemistry, PhD thesis, Univ. of Toronto, Canada.

Henrich, R., K.-H. Baumann, R. Huber, and H. Meggers (2002), Carbonate preservation records of the past 3 Myr in the Norwegian–Greenland Sea and the northern North Atlantic: Implications for the history of NADW production, *Deep Sea Res., Part I*, *184*(1–2), 17–39, doi:10.1016/S0025-3227(01)00279-1.

Jaiser, R., K. Dethloff, D. Handorf, A. Rinke, and J. Cohen (2012), Impact of sea ice cover changes on the Northern Hemisphere atmospheric winter circulation, *Tellus A*, *64*(0), 497, doi:10.1029/2010GL045698.

Jansen, E., and J. Sjøholm (1991), Reconstruction of glaciation over the past 6 Myr from ice-borne deposits in the Norwegian Sea, *Nature*, *349*(6310), 600–603, doi:10.1038/349600a0.

Jansen, E., U. Bleil, R. Henrich, L. Kringstad, and B. Slettemark (1988), Paleoenvironmental changes in the Norwegian Sea and the northeast Atlantic during the last 2.8 m.y: Deep Sea Drilling Project/Ocean Drilling Program Sites 610, 942, 943, and 644, *Paleoceanography*, *3*(5), 563–581, doi:10.1029/PA003i005p00563.

Jansen, E., T. Fronval, F. Rack, and J. E. T. Channell (2000), Pliocene–Pleistocene ice rafting history and cyclicity in the Nordic Seas during the last 3.5 Myr, *Paleoceanography*, *15*(6), 709–721, doi:10.1029/1999PA000435.

Kleiven, H. F., E. Jansen, T. Fronval, and T. Smith (2002), Intensification of Northern Hemisphere glaciations in the circum Atlantic region (3.5–2.4 Ma) – Ice-rafted detritus evidence, *Palaeogeogr. Palaeoclimatol. Palaeoecol.*, *184*(3–4), 213–223, doi:10.1016/S0031-0182(01)00407-2.

Klocker, A., M. Prange, and M. Schulz (2005), Testing the influence of the Central American Seaway on orbitally forced Northern Hemisphere glaciation, *Geophys. Res. Lett.*, *32*, L03703, doi:10.1029/2004GL021564.

Kucera, M. (2007), Planktonic foraminifera as tracers of past oceanic environments, in *Proxies in Late Cenozoic Paleoceanography*, vol. 1, edited by C. Hillaire-Marcel and A. de Vernal pp. 213–262, Elsevier, Rotterdam, doi:10.1016/S1572-5480(07)01011-1.

Kucera, M., et al. (2005), Reconstruction of sea-surface temperatures from assemblages of planktonic foraminifera: Multi-technique approach based on geographically constrained calibration data sets and its application to glacial Atlantic and Pacific Oceans, *Quat. Sci. Rev.*, *24*, 951–998, doi:10.1016/j.quascirev.2004.07.014.

Kuhlmann, G., C. Langereis, D. Munsterman, R. J. van Leeuwen, R. Verreussel, J. Meulenkamp, and T. Wong (2006a), Chronostratigraphy of Late Neogene sediments in the southern North Sea Basin and paleoenvironmental interpretations, *Palaeogeogr. Palaeoclimatol. Palaeoecol.*, *239*, 426–455, doi:10.1016/j.palaeo.2006.02.004.

Kuhlmann, G., C. Langereis, D. Munsterman, R.-J. van Leeuwen, R. Verreussel, J. E. Meulenkamp, and T. E. Wong (2006b), Integrated chronostratigraphy of the Pliocene–Pleistocene interval and its relation to the regional stratigraphical stages in the southern North Sea region, *Geol. Mijnbouw*, *85–1*, 19–35.

Lisiecki, L. E., and M. E. Raymo (2005), A Pliocene–Pleistocene stack of 57 globally distributed benthic δ^{18}O records, *Paleoceanography*, *20* PA1003, doi:10.1029/2004PA001071.

Lisiecki, L. E., and M. E. Raymo (2007), Plio-Pleistocene climate evolution: Trends and transitions in glacial cycle dynamics, *Quat. Sci. Rev.*, *26*, 56–69, doi:10.1016/j.quascirev.2006.09.005.

Liu, T., and Z. Ding (1998), Chinese loess and the paleomonsoon, *Annu. Rev. Earth Planet. Sci.*, *26*, 111–145, doi:10.1146/annurev.earth.26.1.111.

Locarnini, R. A., A. V. Mishonov, J. I. Antonov, T. P. Boyer, and H. E. Garcia (2010), *World Ocean Atlas 2009 Volume 1: Temperature in NOAA Atlas NESDIS*, vol. 68, edited by S. Levitus, 184 pp., U.S. Government Printing Office, Washington, D. C.

Lu, R., and B. Dong (2008), Response of the Asian summer monsoon to weakening of Atlantic thermohaline circulation, *Adv. Atmos. Sci.*, *25*(5), 723–736, doi:10.1007/s00376-008-0723-z.

Lunt, D. J., G. L. Foster, A. M. Haywood, and E. J. Stone (2008a), Late Pliocene Greenland glaciation controlled by a decline in atmospheric CO_2 levels, *Nature*, *454*(7208), 1102–1106, doi:10.1038/nature07223.

Lunt, D. J., P. J. Valdes, A. M. Haywood, and I. C. Rutt (2008b), Closure of the Panama Seaway during the Pliocene: Implications for climate and Northern Hemisphere glaciation, *Clim. Dyn.*, *30*(1), 1–18, doi:10.1007/s00382-007-0265-6.

Mashiotta, T. A., D. W. Lea, and H. J. Spero (1999), Glacial–interglacial changes in sub-Antarctic sea surface temperature and δ^{18}O-water using foraminiferal Mg, *Earth Planet. Sci. Lett.*, *170*(4), 417–432, doi:10.1016/S0012-821X(99)00116-8.

Maslin, M. A., X. S. Li, M.-F. Loutre, and A. Berger (1998), The contribution of orbital forcing to the progressive intensification of Northern Hemisphere glaciation, *Quat. Sci. Rev.*, *17*, 411–426, doi:10.1016/S0277-3791(97)00047-4.

McCartney, M. S., and C. Mauritzen (2001), On the origin of the warm inflow to the Nordic Seas, *Progr. Oceanogr.*, *51*(1), 125–214, doi:10.1016/S0079-6611(01)00084-2.

McCartney, M. S., and L. D. Talley (1982), The subpolar mode water of the North Atlantic Ocean, *J. Phys. Oceanogr.*, *12*(11), 1169–1188, doi:10.1175/1520-0485(1982)012 < 1169:TSMWOT > 2.0.CO;2.

Naafs, B. D. A., R. Stein, J. Hefter, N. Khelifi, S. De Schepper, and G. H. Haug (2010), Late Pliocene changes in the North Atlantic Current, *Earth Planet. Sci. Lett.*, *298*, 434–442, doi:10.1016/j.epsl.2010.08.023.

Naafs, B. D. A., J. Hefter, G. Acton, G. H. Haug, A. Martínez-Garcia, R. Pancost, and R. Stein (2012), Strengthening of North American dust sources during the late Pliocene (2.7 Ma), *Earth Planet. Sci. Lett.*, *317–318*, 8–19.

Naafs, B. D. A., J. Hefter, and R. Stein (2013a), Millennial-scale ice rafting events and Hudson Strait Heinrich(-like) Events during the late Pliocene and Pleistocene: A review. *Quat. Sci. Rev.*, *80*, 1–18, doi:10.1016/j.quascirev.2013.08.014.

Naafs, B. D. A., J. Hefter, J. Grützner, and R. Stein (2013b), Warming of surface waters in the mid-latitude North Atlantic during Heinrich events. *Paleoceanography*, *28*, 153–163, doi:10.1029/2012PA002354, 2013.

Nürnberg, D., and J. Groeneveld (2006), Pleistocene variability of the Subtropical Convergence at East Tasman Plateau: Evidence from planktonic foraminiferal Mg/Ca (ODP Site 1172A), *Geochem. Geophys. Geosyst.*, *7*, Q04P11, doi:10.1029/2005GC000984.

Pagani, M., Z. Liu, J. LaRiviere, and A. C. Ravelo (2010), High Earth-system climate sensitivity determined from Pliocene carbon dioxide concentrations, *Nat. Geosci.*, *3*(1), 27–30, doi:10.1038/NGEO724.

Paillard, D. (1996), Macintosh program performs time-series analysis, *Eos Trans. AGU*, *77*(39), 379–385, doi:10.1029/96EO00259.

Penaud, A., F. Eynaud, J. L. Turon, S. Zaragosi, F. Marret, and J. F. Bourillet (2008), Interglacial variability (MIS 5 and MIS 7) and dinoflagellate cyst assemblages in the Bay of Biscay (North Atlantic), *Mar. Micropaleontol.*, *68*, 136–155, doi:10.1016/j. marmicro.2008.01.007.

Pflaumann, U., et al. (2003), Glacial North Atlantic: Sea-surface conditions reconstructed by GLAMAP 2000, *Paleoceanography*, *18*(3), 1065, doi:10.1029/2002PA000774.

Prange, M., and M. Schulz (2004), A coastal upwelling seesaw in the Atlantic Ocean as a result of the closure of the Central American Seaway, *Geophys. Res. Lett.*, *31*, L17207, doi:10.1029/2004GL020073.

Rasmussen, T. L., and E. Thomsen (2004), The role of the North Atlantic Drift in the millennial timescale glacial climate fluctuations, *Palaeogeogr. Palaeoclimatol. Palaeoecol.*, *210*(1), 101–116, doi:10.1016/j.palaeo.2004.04.005.

Ravelo, A. C., and D. Andreasen (2000), Enhanced circulation during a warm period, *Geophys. Res. Lett.*, *27*(7), 1001–1004, doi:10.1029/1999GL007000.

Ravelo, A. C., and C. Hillaire-Marcel (2007), The use of oxygen and carbon isotopes of foraminifera in paleoceanography, in *Proxies in Late Cenozoic Paleoceanography*, vol. 1, edited by C. Hillaire-Marcel and A. de Vernal, pp. 735–764, Elsevier, Rotterdam, doi:10.1016/S1572-5480(07)01023-8.

Ravelo, A. C., D. H. Andreasen, M. Lyle, A. O. Lyle, and M. W. Wara (2004), Regional climate shifts caused by gradual global cooling in the Pliocene epoch, *Nature*, *429*(6989), 263–267, doi:10.1038/nature02567.

Raymo, M. E. (1994), The initiation of Northern Hemisphere glaciation, *Annu. Rev. Earth Planet. Sci.*, *22*, 353–383, doi:10.1146/annurev. ea.22.050194.002033.

Raymo, M. E., and K. Nisancioglu (2003), The 41 kyr world: Milankovitch's other unsolved mystery, *Paleoceanography*, *18*(1), 1011, doi:10.1029/ 2002PA000791.

Raymo, M. E., D. Hodell, and E. Jansen (1992), Response of Deep Ocean Circulation to Initiation of Northern Hemisphere Glaciation (3–2 Ma), *Paleoceanography*, *7*(5), 645–672, doi:10.1029/92PA01609.

Raymo, M. E., L. E. Lisiecki, and K. H. Nisancioglu (2006), Plio-Pleistocene ice volume, Antarctic climate, and the global δ^{18}O record, *Science*, *313*(5786), 492–495, doi:10.1126/science.1123296.

Raymo, M. E., and W. F. Ruddiman (1992), Tectonic forcing of late Cenozoic climate, *Nature*, *359*(6391), 117–122, doi:10.1038/359117a0.

Raymo, M. E., W. F. Ruddiman, J. Backman, B. M. Clement, and D. G. Martinson (1989), Late Pliocene variation in Northern Hemisphere ice sheets and North Atlantic deep water circulation, *Paleoceanography*, *4*(4), 413–446, doi:10.1029/PA004i004p00413.

Rea, D. K., and H. Schrader (1985), Late Pliocene onset of glaciation: Ice-rafting and diatom stratigraphy of North Pacific DSDP cores, *Palaeogeogr. Palaeoclimatol. Palaeoecol.*, *49*(3–4), 313–325, doi:10.1016/0031-0182(85)90059-8.

Reynolds, B. C., M. Frank, and A. N. Halliday (2008), Evidence for a major change in silicon cycling in the subarctic North Pacific at 2.73 Ma, *Paleoceanography*, *23*, PA4219, doi:10.1029/2007PA001563.

Robinson, M. M., H. J. Dowsett, G. S. Dwyer, and K. T. Lawrence (2008), Reevaluation of mid-Pliocene North Atlantic sea surface temperatures, *Paleoceanography 23*, PA3213, doi: 10.1029/2008PA001608.

Rochon, A., A. de Vernal, J.-L. Turon, J. Matthiessen, and M. J. Head (1999), Distribution of recent dinoflagellate cysts in surface sediments from the North Atlantic Ocean and adjacent seas in relation to sea-surface parameters, *AASP Contrib. Ser.*, *35*, 1–152.

Rohling, E. J. (2007), Progress in paleosalinity: Overview and presentation of a new approach, *Paleoceanography*, *22*, PA3215, doi:10.1029/ 2007PA001437.

Ruddiman, W. F., R. B. Kidd, E. Thomas, and Shipboard Scientific Party Leg 94 (1987a), Site 607, *Proc. Deep Sea Drill. Project Init. Rep.*, *94*, 75–147, doi:10.2973/dsdp.proc.94.103.1987.

Ruddiman, W. F., R. B. Kidd, E. Thomas, and Shipboard Scientific Party Leg 94 (1987b), Site 610, *Proc. Deep Sea Drill. Project Init. Rep.*, *94*, 351–470, doi:10.2973/dsdp.proc.94.106.1987.

Schiebel, R., J. Bijma, and C. Hemleben (1997), Population dynamics of the planktic foraminifer *Globigerina bulloides* from the eastern North Atlantic, *Deep Sea Res., Part I*, *44*(9), 1701–1713, doi:10.1016/S0967-0637(97)00036-8.

Schlitzer, R., (2011), Ocean data view. [Available at http://odv.awi.de.]

Seki, O., G. L. Foster, D. N. Schmidt, A. Mackensen, K. Kawamura, and R. D. Pancost (2010), Alkenone and boron-based Pliocene pCO$_2$ records, *Earth Planet. Sci. Lett.*, *292*(1–2), 201–211, doi:10.1016/j.epsl.2010.01.037.

Shackleton, N. J. (1974), Attainment of isotopic equilibrium between ocean water and benthonic foraminifera genus *Uvigerina*: Isotopic changes in the ocean during the last glacial, *Colloq. Int. C. N. R. S.*, *219*, 203–210.

Shackleton, N. J., et al. (1984), Oxygen isotope calibration of the onset of ice-rafting and history of glaciation in the North Atlantic region, *Nature*, *307*(5952), 620–623, doi:10.1038/307620a0.

Sigman, D. M., S. L. Jaccard, and G. H. Haug (2004), Polar ocean stratification in a cold climate, *Nature*, *428*(6978), 59–63, doi:10.1038/nature02357.

Stockmarr, J. (1971), Tablets with spores used in absolute pollen analysis, *Pollen et Spores*, *13*, 615–621.

Stoker, M. S., D. Praeg, B. O. Hjelstuen, J. S. Laberg, T. Nielsen, and P. M. Shannon (2005), Neogene stratigraphy and the sedimentary and oceanographic development of the NW European Atlantic margin, *Mar. Petrol. Geol.*, *22*, 977–1005, doi:10.1016/j.marpetgeo.2004.11.007.

Stramma, L. (2001), Current systems in the Atlantic Ocean, in *Encyclopedia of Ocean Sciences*, edited by S. A. Thorpe and K. Turekian, pp. 589–598, Academic Press, San Diego, Calif.

Suc, J.-P., and W. H. Zagwijn (1983), Plio–Pleistocene correlations between the northwestern Mediterranean region and northwestern Europe according to recent biostratigraphic and palaeoclimatic data, *Boreas*, *12*, 153–166.

Sy, A. (1988), Investigation of large-scale circulation patterns in the central North Atlantic: The North Atlantic current, the Azores Current, and the Mediterranean Water Plume in the area of the Mid-Atlantic ridge, *Deep Sea Res. Part A*, *35*(3), 383–413, doi:10.1016/0198-0149(88)90017-9.

Thierens, M., E. Browning, H. Pirlet, M.-F. Loutre, B. Dorschel, V. A. I. Huvenne, J. Titschack, C. Colin, A. Foubert, and A. J. Wheeler (2013), Cold-water coral carbonate mounds as unique palaeo-archives: The Plio–Pleistocene Challenger Mound record (NE Atlantic), *Quat. Sci. Rev.*, *73*(0), 14–30, doi: 10.1016/j.quascirev.2013.05.006.

Versteegh, G. J. M. (1994), Recognition of cyclic and non-cyclic environmental changes in the Mediterranean Pliocene: A palynological approach, *Mar. Micropaleontol.*, *23*(2), 147–183, doi:10.1016/0377-8398(94)90005-1.

Versteegh, G. J. M. (1997), The onset of major Northern Hemisphere glaciations and their impact on dinoflagellate cysts and acritarchs from the Singa section, Calabria (southern Italy) and DSDP Holes 607/607A (North Atlantic), *Mar. Micropaleontol.*, *30*(4), 319–343, doi:10.1016/ S0377-8398(96)00052-7.

Versteegh, G. J. M., and K. A. F. Zonneveld (1994), Determination of (palaeo-)ecological preferences of dinoflagellates by applying detrended and canonical correspondence-analysis to Late Pliocene dinoflagellate cyst assemblages of the South Italian Singa section, *Rev. Palaeobot. Palyno.*, *84*, 181–199, doi:10.1016/0034-6667(94)90050-7.

HENNISSEN ET AL.   16

Versteegh, G. J. M., H. Brinkhuis, H. Visscher, and K. A. F. Zonneveld (1996), The relation between productivity and temperature in the Pliocene North Atlantic at the onset of Northern Hemisphere glaciation: A palynological study, *Global Planet. Change*, *11*(4), 155–165, doi:10.1016/0921-8181(95)00054-2.

Vincent, E., and W. H. Berger (1981), Planktonic foraminifera and their use in paleoceanography, in *The Oceanic Lithosphere. The Sea*, edited by C. Emiliani, vol. 7, pp. 1025–1119, Wiley-Interscience, Hoboken, N. J.

Vorren, T. O., M. Hald, and E. Lebesbye (1988), Late Cenozoic environments in the Barents Sea, *Paleoceanography*, *3*(5), 601–612, doi:10.1029/PA003i005p00601.

Wall, D., and B. Dale (1966), "Living fossils" in western Atlantic plankton, *Nature*, *211*, 1025–1026.

Wall, D., B. Dale, G. P. Lohmann, and W. K. Smith (1977), The environmental and climatic distribution of dinoflagellate cysts in modern marine sediments from regions in the North and South Atlantic Oceans and adjacent seas, *Mar. Micropaleontol.*, *2*, 121–200, doi:10.1016/0377-8398(77)90008-1.

Warny, S., R. A. Askin, M. J. Hannah, B. A. R. Mohr, J. I. Raine, D. M. Harwood, F. Florindo, and the SMS Science Team (2009), Palynomorphs from a sediment core reveal a sudden remarkably warm Antarctica during the middle Miocene, *Geology*, *37*(10), 955–958, doi:10.1130/G30139A.1.

Williams, M., A. M. Haywood, E. M. Harper, A. L. A. Johnson, T. Knowles, M. J. Leng, D. J. Lunt, B. Okamura, P. D. Taylor, and J. Zalasiewicz (2009), Pliocene climate and seasonality in North Atlantic shelf seas, *Philos. T. R. Soc. A.*, *367*(1886), 85–108, doi:10.1098/rsta.2008.0224.

Zagwijn, W. H. (1985), An outline of the Quaternary stratigraphy of the Netherlands, *Geol. Mijnbouw*, *64*, 17–24.

Zonneveld, K. A. F., et al. (2013), Atlas of modern dinoflagellate cyst distribution based on 2405 data points, *Rev. Palaeobot.*, *191*, 1–197, doi:10.1016/j.revpalbo.2012.08.003.